Thermal dependent properties of LaB_6-MeB_2 eutectic composites

T.O. Soloviova[a], O.P. Karasevskaa[b], J. Vleugels[c], P.I. Loboda[a]

[a]National Technical University of Ukraine "Igor Sikorsky Kyiv Polytechnic Institute", Peremohy Av. 37, 03680, Kyiv, Ukraine
[b]G.V. Kurdyumov Institute for Metal Physics of the N.A.S. of Ukraine, 36 Vernadsky Boulevard, Kyiv, 03142, Ukraine
[c]KU Leuven, Kasteelpark Arenberg 44, B-3001, Heverlee, Belgium
Corresponding author: tsolov@iff.kpi.ua (T.O. Soloviova).

Abstract The thermal expansion of polycrystalline LaB_6-MeB_2 ceramic composites (where Me denotes Ti, Zr, Hf) has been studied experimentally within the temperature range from 20°C to 1500°C. These ceramic composites were obtained by crucible-free float zone melting method. The first temperature interval with a negative thermal elongation (NTE) (~1000-1100°C) coincided in the LaB_6-MeB_2 composites and LaB_6 hexaboride and was associated with La-La atomic bond softening. The hierarchy of the interatomic Me-Me-B-B bonds in the LaB_6-MeB_2 composite compounds, their interface and residual stresses in the LaB_6 matrix and the MeB_2 reinforcing phase were identified to be the source of such phenomenon. The strong covalent component of interatomic bonds compresses the crystal lattice of the composites after softening ionic and metallic components and removing residual stresses. The composites exhibited several additional NTE intervals at a higher temperature (~1000-1250°C) which were associated with the of interatomic bonds softening in the TiB_2, HfB_2, ZrB_2 reinforcing fibers. NTE intervals determines transition of the deformation mechanism of composites from low-temperature to high-temperature one. Insignificant plasticity and brittle fracture in the area of low-temperature deformation is replaced with an increase in both plasticity and strength with temperature rise.

1. Introduction

High thermionic properties of LaB_6 pure single crystals are widely used, but their applications are limited due to their insufficient mechanical properties and processing problems i.e., brittleness, sensitivity to heating rate, the difficulty of making intricate shapes, small specimens and the like [1-3]. Mechanical properties of LaB_6 single-crystal can be improved by creating LaB_6-MeB_2 composite materials, where Me denotes a Ti, Zr and Hf transition metal. The borides of these metals have a unique combination of mechanical and physical properties, among them including high melting point (>3000 °C), electrical conductivity, thermal resistance and high hardness (25-35 GPa at room temperature) [1,3,4,5]. MeB_2 borides in the form of fibers have the strongest influence on the properties of hexaboride. LaB_6-MeB_2 composites can be obtained a by crucible free float zone melting (FZM) with formation of a coherent interface between the LaB_6 matrix and the MeB_2 fibers. The interatomic bonds in LaB_6 and MeB_2 have metallic, covalent and ionic components and form a strong hierarchy of interatomic interaction with a pronounced crystallographic orientation [6-12]. These borides have a different coefficient of thermal expansion (CTE) and modulus of elasticity. Consequently, residual thermal stresses (RS) arising during the crystallization of the composite, as well as under operating conditions, can provoke the formation of cracks.

The hexaboride crystal structure of rare-earth metals (ReB_6, Re = Y, La, Gd, Tb, Dy, etc.) can be considered as an interaction of a metal and boron sublattice, as illustrated in (Fig. 1a) [7-15]. The atomic bonding between the boron atoms in the octahedron (B–B1) differs, but its strength exceeds the bonding strength between the boron sublattices (B–B2) and is an order of magnitude higher than the bond strength between the metal ions (Fig. 1a), which are "locked" inside the cavities of the (B6) boron octahedron sublattice. Due to the strong covalent bonds of boron atoms in the boron octahedrons, they can be considered as a single structural unit and are commonly replaced by a B* superatom, equal in

mass to the sum of the masses of the constituent boron atoms (B_6 = B*). As a result, the crystal structure of ReB_6 is simplified to the ordinary ReB* cubic structure similar to CsCl. Theoretical and experimental studies have demonstrated an anomalous softening of the vibration modes with a change in temperature and pressure in several directions of the Brillouin zone, which is manifested by an instability of the ReB* crystal lattice. For lanthanum hexaboride, atomic bond softening was observed experimentally [11] and theoretically [8,9,15], initially in the <111> direction around ~1050°C, and in the <100> and <110> directions at a higher temperature. The Debye temperature in LaB_6 polycrystals is assumed to be within the range ~1060-1200°C [16,17].

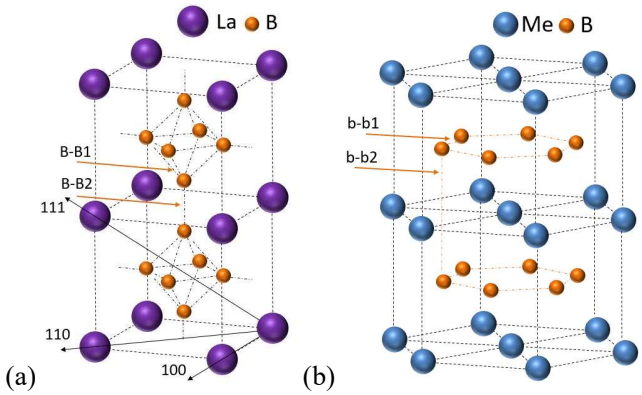

Fig. 1. Crystal structures of LaB_6 (a) and MeB_2 (b): a) B-B1 – the bonding between boron atomics in the octahedron, B-B2 – the bonding between the octahedrons (the boron sublattices), b) b-b1 – the bonding between boron atomics in the boron networks; b-b2 – the bonding between boron networks.

In MeB_2 diborides, there is a hierarchy of interatomic bonding also [6,18-22]. Boron atoms form planar networks that have crystallographic directed covalent bonds b-b1, b-b2 and less Me-B interaction (Fig. 1b). In the MeB_2 hexagonal lattice, the b-b1 bond in the boron networks determines the bonding strength along the "a" axis, whereas the stronger b-b2 bonds control the bonding along the "c" axis. This determines c/a lattice parameters ratio as ~1.1 [18-20]. The CTE experimental values in the "a" and "c" directions differ by a factor 2 or more [21,23,24]. Interatomic bonds different nature in LaB_6 matrix and in the MeB_2 reinforcing phase complicates the prediction of the high-temperature properties of LaB_6-MeB_2 composites, what is necessary for their successful application. The objective of this paper effort is to determine an experimental thermal expansion of LaB_6-MeB_2 polycrystalline ceramic composites after FZM and to explain peculiarities of their deformation.

2. Materials and study methods

LaB_6 - 11 wt% TiB_2, LaB6 - 21 wt% ZrB_2, LaB_6 - 30 wt% HfB_2 (purity 98 wt%, average grain size 1 μm, Reaktiv Co Donetsk, Ukraine) powder mixtures were prepared in accordance with their eutectic composition [3,5,25]. The powders were mixed by sifting them 10 times through a 100 μm mesh. 15 ml of a 2.5 wt% polyvinyl alcohol aqueous solution per 100 g of powder mixture was used as binder. To facilitate purification of the starting powder mixture during FZM, 2 vol% amorphous boron (purity 99.8 wt %, particle size 0.5 mm, Reaktiv Co Donetsk, Ukraine) powder was admixed. Boron in the recovery process forms oxides with low melting point and high vapor pressure at 1200°C and therefore can be effectively eliminated from the interaction zone by evaporation followed with condensation on cold walls, excluding the possibility of occurrence of the reverse oxidation reaction. Green rods with a diameter of 10 mm and length of 145 mm were obtained by compressing the mixture in a hydraulic press at 100 MPa. FZM was performed at a rate of 3 mm/min in the "Crystal 206" (Russia) induction equipment in a 0.1 MPa helium environment using a LaB_6 polycrystalline substrate. More details on the processing method are described in [3,26-28].

The crystals were sliced normal ($D^{\perp}$) and parallel ($D\|$) to the FZM growth direction by electrical discharge machining. For dilatometry investigations, the LaB_6-MeB_2 crystals were cut perpendicular to the growth direction into cylindrical samples (diameter is 8-10 mm and length is 8-25 mm). The samples were ground and polished with diamond paste. The thermal expansion studies were performed in Ar+5 vol % H_2 up to 1500°C using a dilatometer (Netzsch DIL 402 C). Alumina was used for dilatometer calibration. The heating and reheating rates were fixed at 5°C/min to ensure a homogeneous temperature distribution within the sample. The thermal expansion of the samples was calculated using experimental relative elongation data [23]. Microstructural investigation of the composites was performed by scanning microscopy (SEM, XL30-FEG, FEI, The Netherlands). Three X-ray diffraction (XRD) methods: θ-2θ scanning, pole figures and RSM (reciprocal space mapping) were used to analyze phase states, crystallographic texture, and composite substructure. X-ray studies were performed in monochromatic CuK_{α} radiation on an Ultima IV diffractometer (Rigaku, Japan). The phase states of borides were determined from XRD patterns obtained by "θ-2θ" scanning with a step of 0.02° and a measurement time of 4 s/step in the Bragg-Brentano reflection geometry. The calculation was carried out using software based on the Rietveld method developed by Rigaku. Pole figures were determined for {110} LaB_6 reflections using the Schultz back-reflection technique. In the RSM method, the sample was successively displaced with a step of 0.01° along two mutually perpendicular axes (ω1 and ω2) with an exposure of 2 s/step. The intensity ($Iq_{\perp}$) and width ($\omega q_{\perp n}$) distribution of the RSM diffraction spots in the azimuthally plane depend on the homogeneity, type, density and the location of dislocations in a material and change depending on direction according to [29]:

$$\omega_{q\perp n} \sim \sum_i \rho_i \phi_{in}(b_i, \tau_i, q) \quad (1)$$

where b_i is the Burgers vector of a dislocation from the i^{th} slip system; ρ_i is the dislocation density; τ_i is the orientation of dislocation lines; φ_{in} is the orientation factor, q is the diffraction vector. Accuracy of angular distribution spots is 5′-9′ with a 0.95 confidence probability.

3. Results and discussion

3.1. Microstructure and phase state of ceramics after FZM

Typical microstructures of LaB_6 and LaB_6-MeB_2 polycrystalline ceramics after FZM are shown in Fig. 2. LaB_6 microstructure is of oblong coarse-grained shape with an average diameter of 0.3-0.6 mm for $D^{\perp}$ and 1.2-1.5 mm for $D\|$ (Fig. 2a and b). LaB_6 microstructure along $D\|$ (Fig. 2b) shows some grains wedged out along the sample axis. Etching pits (Fig. 2c) indicate the existence of subboundaries and the separation of grains into elongated subgrains. The size of subgrains is in two orders smaller than the grain size.

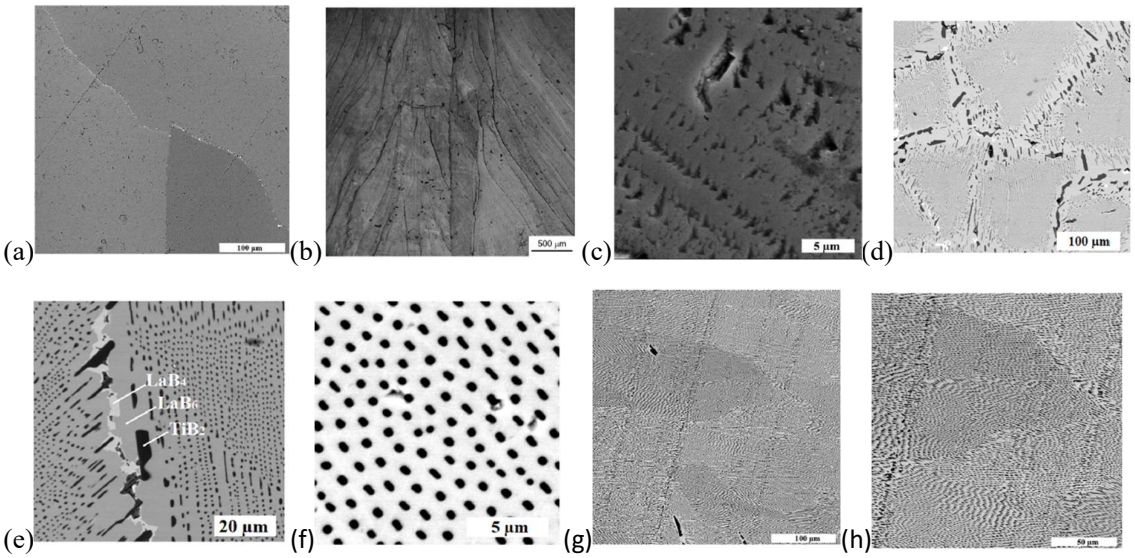

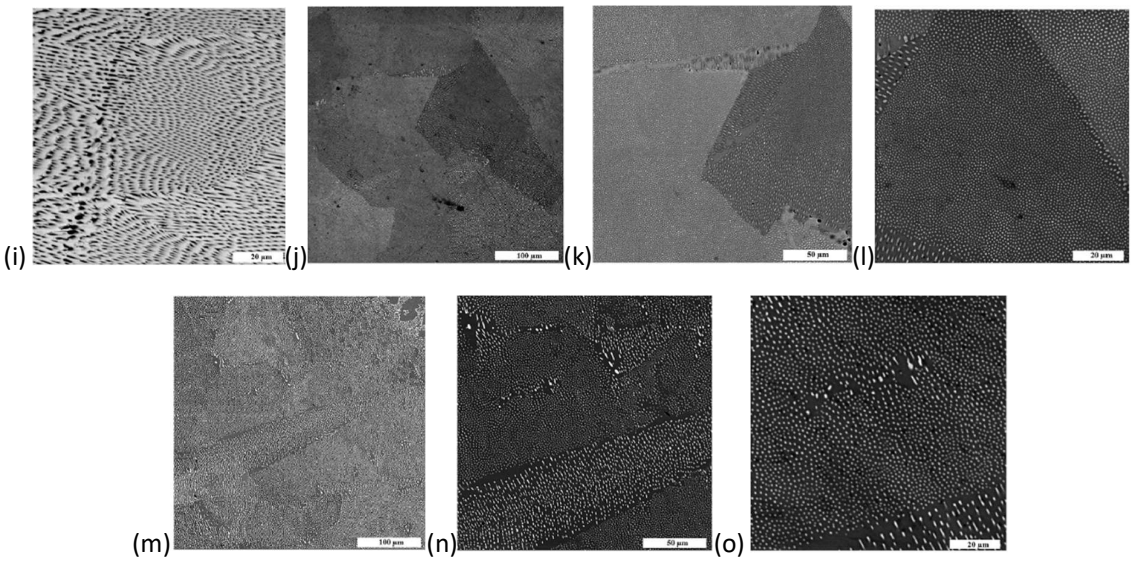

Fig. 2. Typical microstructure of polycrystalline LaB_6 (a, b, c) and LaB_6-MeB_2 borides (d-o). LaB_6-TiB_2 - d, e, f, g, h, i; LaB_6-HfB_2 - j, k, l; LaB_6-ZrB_2 - m, n, o. Transverse (a, d, e, f, j, k, l, m, n, o) and longitudinal (b, c, g, h, i) sections relative to the direction of growth.

LaB_6-MeB_2 microstructures consists of LaB_6 matrix grains and MeB_2 reinforcing fibers, as shown in Fig. 2d-o. The microstructure of the matrix grains of the LaB_6-MeB_2 composites and the LaB_6 ceramics are similar. LaB_6 grains in LaB_6-MeB_2 composites have a columnar shape, but with smaller sizes in the $D^{\perp}$ (0.07-0.2 mm) (Fig. 2d and e, j, k, m, n) and D|| (0.7-1.1 mm) (Fig. 2g and h) cross-sections as compared to grains in LaB_6. The MeB_2 fibers diameter (Fig. 2f, i, l, o) is 0.3-0.7 μm, and the distance between them is determined by their concentration in the composite. In the LaB_6-TiB_2 composite, the distance between the fibers is 2-10 μm, for LaB_6-ZrB_2 and LaB_6-HfB_2 composites this distance is about 2 and 1.5 times smaller, i.e. 3-6 μm and 4-8 μm, respectively. In general, the structures of LaB_6-MeB_2 composites are morphologically similar, and fibers size differences are associated with different concentrations and diffusion rates of the La, Ti, Zr, Hf, B components at the crystallization front.

Sometimes, in addition to the LaB_6 and MeB_2 phases, the LaB_4 phase can be observed (Fig. 2e). Most often in LaB_6-MeB_2 composites, the following crystallographic relationships between matrix and fibers are identified: <001> LaB_6//[001] MeB_2, {110} LaB_6//(110) MeB_2, or <111> LaB_6//[001] MeB_2 and {110} LaB_6//(11¯ 0) MeB_2 [5,25,30].

For cross-sections LaB_6 and LaB_6-MeB_2 the XRD patterns are shown in Fig. 3a, c, e, g. The XRD pattern of LaB_6 ceramics corresponds to the polycrystalline state with a lattice parameter of 0.4156 nm (as in PDF-LaB6-01-073-1669 ICDD). The XRD patterns of the LaB_6-MeB_2 ceramics are multicomponent and, according to the Rietveld analysis, contain 11-12 wt% TiB_2, 20-22 wt% ZrB_2 and 28–30 wt% HfB_2 reinforcing phase in the LaB_6-TiB_2, LaB_6-ZrB_2 and LaB_6-HfB_2, respectively in agreement with the equilibrium phase diagrams [3,5,25]. Metallographic investigation of the LaB_6-MeB_2 ceramics clearly shows their eutectic nature correspond to the data for the boride components with an accuracy of 99.99% (ICDD's PDF-TiB_2-01-089-3923, PDF-ZrB_2-00-034-0423 and PDF-HfB_2-00-038-1398). In addition to the eutectic phases, the LaB_6-MeB_2 composites contained 4-7 wt % non-equilibrium phases. Among them is the LaB_4 phase (~2-3 wt%). Other non-equilibrium phases, which due to the small number of low-intensity reflections can be considered unknown, are close in terms of the lattice parameter to $LaB_{6\pm x1}$ and $MeB_{2\pm x2}$, where x_1 and x_2 are less than 1 [27,28].

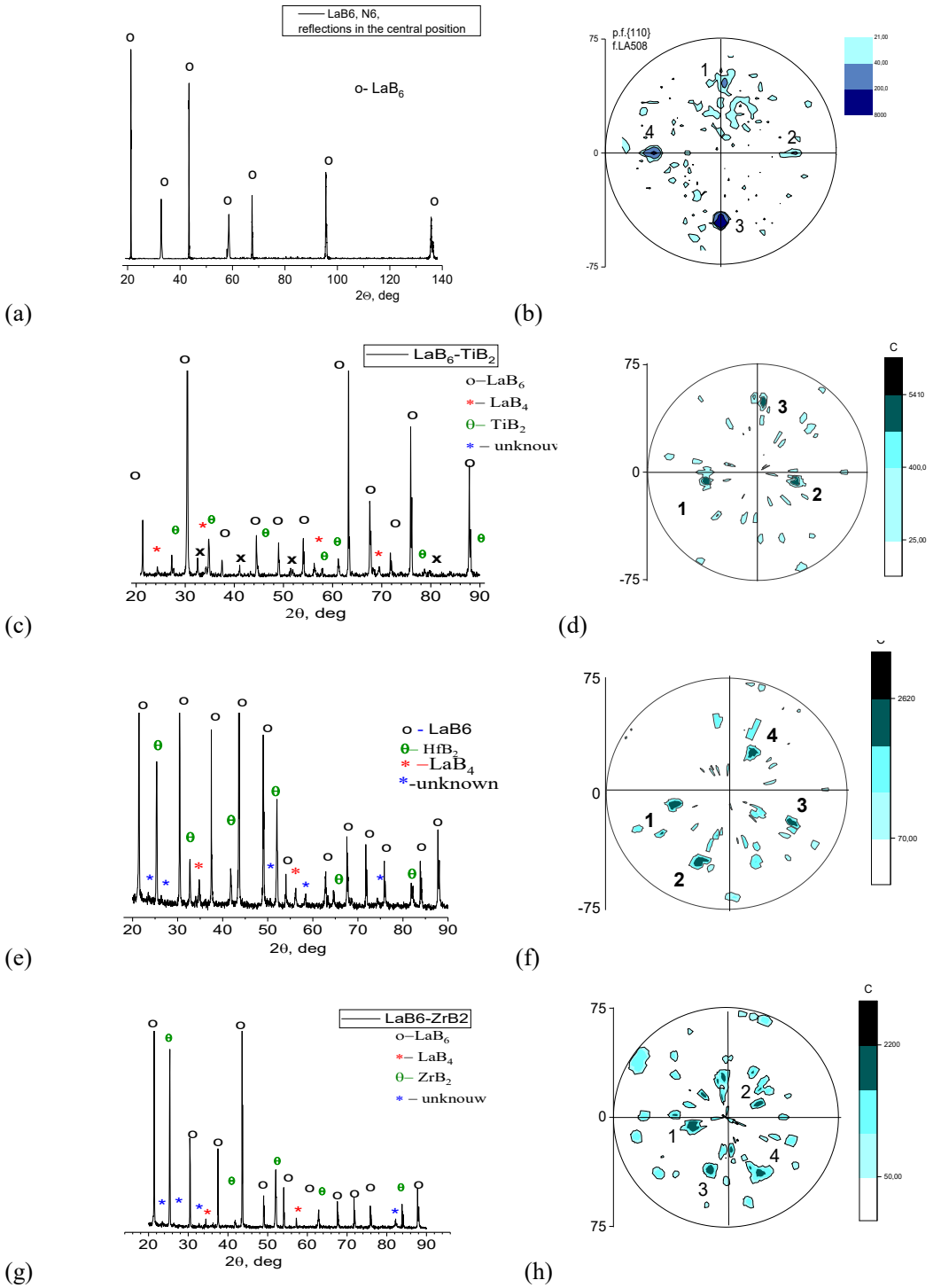

Fig. 3. XRD patterns (a, c, e, g) and {110} pole figures (b, d, f, h) of the crucible-free FZM LaB_6 and LaB_6-MeB_2 composites, cross-sectioned perpendicular to the growth direction. LaB_6 (a, b), LaB_6-TiB_2 (c, d), LaB_6-HfB_2 (e, f), LaB_6-ZrB_2 (g, h).

The {110} pole figures of the LaB_6 phase in the LaB_6-MeB_2 and LaB_6 ceramics of the cross-section, perpendicular to the motion of the melting zone are shown in Fig. 3b, d, e, h. These pole figures do not indicate a pronounced preferential orientation along the direction of motion of the melting zone.

However, a significant increase in the intensity of some spots was observed in the pole figures in Fig. 3b, d, e, h (Fig. 3h, f, b, spots 1, 2, 3, 4 and, Fig. 3d, spots 1, 2, 3), forming preferred surface plane orientations of samples {001}, {111}, {011} and {011}, respectively. Over a considerable length of FZM samples (~100 mm), these orientations are averaged, and one may assert that composites (and hexaborides) have a polycrystalline textureless state. On short samples with large elongated grains, averaging over orientations does not occur and they have a predominant texture, although not clearly expressed. There is a discrepancy in the textural state of long and short FZM composite samples.

The {hkl} intensities on the XRD patterns of the LaB_6-MeB_2 and LaB_6 ceramics correspond to the presence of grains (or groups of grains) of preferred orientations also. The relative intensities of LaB_6 {hkl}/LaB_6 {110} reflections in LaB_6-MeB_2 and LaB_6 experimental ceramic samples differ many times (in some cases up to ~ 20 times) as their tabular values (PDF-2 01–074-8053 ICDD) for polycrystalline textureless states (Table 1). The difference in the intensity of diffraction patterns after FZM and tabular data confirms the presence of predominant crystallographic orientations in the cross-sections of ceramic samples.

Relatively large, elongated grains, significant temperature gradients along and perpendicular to the direction of motion of the melting zone characterize the FZM process results in a preferred limited crystallographic as well as morphological texture during crystallization. Under the influence of thermal gradients and directions of predominant growth, grains of some crystallographic orientations are wedged out and others appear along the length of the cylindrical specimen [31].

Table 1 The ratio of experimental and tabular intensity values LaB_6{hkl}/LaB_6{110} in the LaB_6 and LaB_6-MeB_2 composites.

Borides	Intensity{hkl}/Intensity {110} of LaB_6 card ICDD, PDF-2 01-074-8053, %						
	{100}/ {110}	{110}/ {110}	{111}/ {110}	{200}/ {110}	{210}/ {110}	{211}/ {110}	{220}/ {110}
LaB_6 ICDD, PDF-2 01-074-8053	0.6	1	0.5	0.2	0.45	0.25	0.10
LaB_6	25	1	0.7	18	0.1	0.1	0.1
LaB_6-TiB_2	0.15	1	0.3	0.15	0.2	0.25	0.8
LaB_6-ZrB_2	3	1	0.9	0.4	0.5	0.6	0.15
LaB_6-HfB_2	2	1	0.85	0.3	0.8	0.25	0.25

3.2. Dilatometry investigations

Dilatation curves ($\Delta l/10 \sim f(T)$) along the axis of 8 mm long LaB_6 sample upon initial and repeated heating are shown in Fig. 4 a. In both cases, the elongation of LaB_6 ceramics in the direction of movement of the melting zone demonstrates almost linear thermal expansion in the temperature range from 20°C to 1500°C. Thermal shrinkage for both samples is observed in the temperature range of 1050-1150°C. This defines a relatively small temperature range for negative thermal elongation (NTE). NTE is less pronounced during initial heating. Above and below the NTE interval, the hexaboride expands linearly with practically the same slope. Upon reheating, NTE is manifested less pronounced, and the values of thermal expansion before and after the NTE interval differ. When hexaboride is reheated, the rectilinear region of $l/10 \sim f(T)$ in the range 1150-1500°C is maintained at a slightly lower value (~0.08%), as compared to the interval below 1000°C.

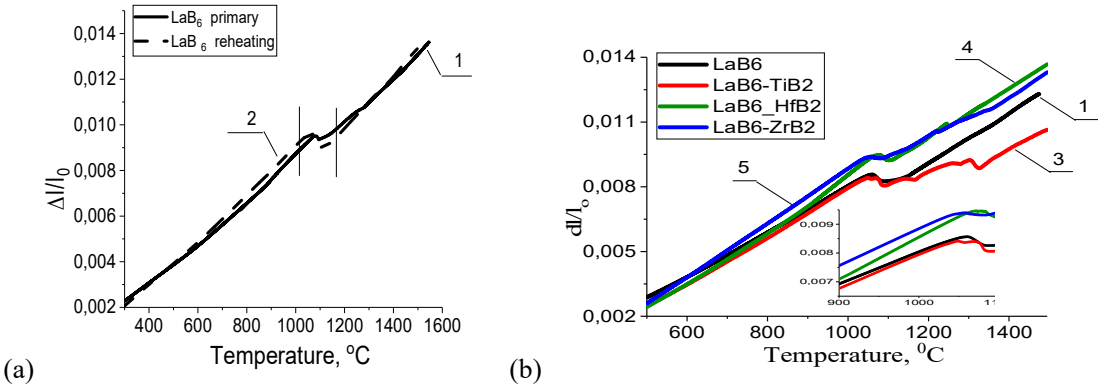

Fig. 4. Dilatometry curves for the FZM polycrystalline LaB_6 (a) and LaB_6-MeB_2 (b); a) curve 1-primary heating, curve 2-reheating b) primary heating of the LaB_6-TiB_2 (curve 3, red), LaB_6-HfB_2 (curve 4, green) and LaB_6-ZrB_2 (curve 5, blue).

Discontinuities in dilatation curves are often associated with phase transformations in a material [32,33]. Since the studied LaB_6 is single-phase and does not have any phase transformations in the temperature range of 20-1400°C [34], other phenomena must be responsible for the discontinuity. The main crystallographic directions <001>, <011>, <111> in this hexaboride have different longitudinal modes of lattice vibrations during heating [7-10]. The vibrations of La-La atoms lying on the <111> diagonal of the crystal lattice are the largest since the shielding effect of the boron octahedron is the strongest in this direction. Schematically, the influence of local vibrational modes responsible for the appearance of NTE can be demonstrated on a simple image (Fig. 5).

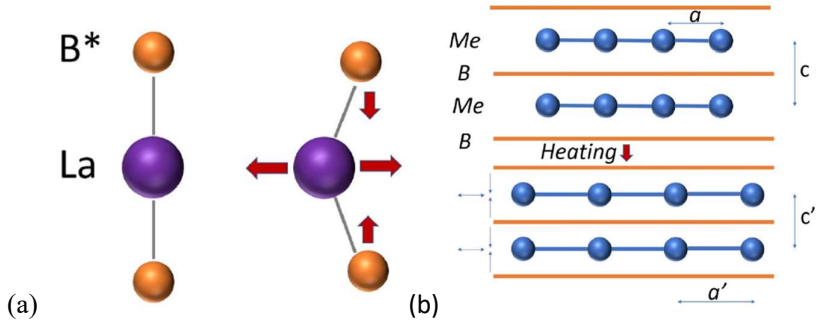

Fig. 5. Representation of the formation of NTE in LaB* (a) and MeB_2 (b) phase components of LaB_6-MeB_2 composites [35,36].

In lanthanum hexaboride, La and B* atoms form a linear bonding only along the <111> directions (Fig. 1, Fig. 5). B* superatom screens the bonding between La atoms in this direction. As the temperature rises, the amplitudes of the La cations vibrations on the <111> diagonals increase, which allows the B* anions to approach each other - the NTE effect appears (Fig. 5). In our opinion, the fuzzy range of NTE values during the first heating of the samples is masked by averaging the softening over random orientation zones of the LaB_6 sample in the absence of a dominant texture. In addition, the indistinctness of the NTE interval is possibly related to the relaxation of bulk RS arising during FZM crystallization. Primary heating of LaB_6 to 1500°C decreases RS [27], while secondary heating makes the NTE interval more evident.

In Fig. 4b the dilatation curves of the short LaB_6-MeB_2 samples during primary heating are shown. The thermal expansion is almost linear in the temperature range of 20-1000°C, similar to that of LaB_6. All composites show a thermal shrinkage comparable to the LaB_6 around 1050-1070°C. This first NTE

temperature range in all LaB_6-MeB_2 composites coincides with the NTE interval of the LaB_6 hexaboride, i.e. the matrix in these composites. Unlike for LaB_6, the composites exhibit additional NTE intervals in the dilatometer curve at temperatures above the first NTE range (Fig. 4b, curves 3, 4, 5). NTE intervals at temperatures above 1150°C can be caused by softening of interatomic bonds in MeB_2 diborides. Boron and metallic atoms (Me) form planar networks with various interatomic bonds in and between these networks (Fig. 5b). With MeB_2 diborides temperature raising, the vibration amplitudes of metal atoms networks with a predominant metallic bond increase. Boride networks with a predominantly stronger covalent bonding can converge (Fig. 2, Fig. 5). The NTE effect appears.

In composites with different types of reinforcing fibers (TiB_2, HfB_2, ZrB_2), the number of NTE intervals and their temperature ranges are different. The highest number of NTE intervals and largest displacement are observed for the LaB_6-TiB_2 composite, whereas less significant NTE was observed for the LaB_6-HfB_2 composite. It is noteworthy that the slope of the dilatometer curve in the range of 20-1000°C and 1250-1500°C depends on the diboride fibers. For one type of fibers, the slope of the dilatometer curve on opposite sides of the NTE intervals (1000-1250°C) differs by ~0.05-0.1%. When the composite specimens are reheated, the dilatometer curve is fundamentally similar to the primary heating (Fig. 6a). For the LaB_6-TiB_2 composite, a linear positive change in elongation is observed in the range of 20-1000°C, the first NTE interval occurs in the region of 1000-1100°C, and then additional NTE intervals, characteristic of the composite material. The slope of the Δl/10~f (T) dependence is maintained at a slightly lower value (0.07-0.10%) in the range 1250-1500°C as compared to the interval below 1000°C.

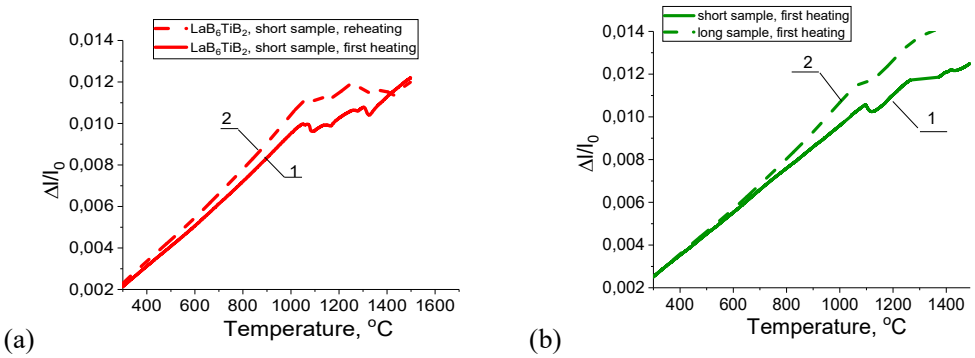

Fig. 6. Dilatometry curves for the primary (1) and reheating (2) samples (a) and short (1) and long (2) samples (b); a) - LaB_6-TiB_2 composite; b) - LaB_6-HfB_2 composite.

Fig. 6b shows the elongations of short (1) and long (2) samples using the LaB_6-HfB_2 composite as an example. In a long sample, the elongation is similar to a short sample. The linear portion (20-1000°C) of the Δl/10~f (T) elongation dependence is preserved. The first NTE interval is in the range of 1050-1150°C, and when this temperature is exceeded, several bends are observed on the Δl/10~f(T) dependence, although their quantity, value and temperature are somewhat different.

In contrast to LaB_6, the LaB_6-MeB_2 composites obtained by FZM contain 5-7 wt% of various non-equilibrium phases, of which 2-3 wt% is LaB_4. The amount of non-equilibrium phases upon heating gradually decreases due to diffusion processes and is accompanied by a continuous change in the lattice parameters of the phase components without discontinuous jumps in the lattice parameters as reported for FZM LaB_6-TiB_2 composites [27]. Thus, the presence of a minor amount of non-equilibrium phases cannot explain the NTE in the dilatometer curves. The phase transition of $LaB_4 + B \rightarrow LaB_6$ occurs only above 1500 °C [34], outside the temperature range studies here, and can therefore not be the cause of the NTE.

3.3. Matrix crystal structure in LaB_6-MeB_2 composites

The intensity distribution $Iq_\perp$ of {100} LaB_6 diffraction spots in LaB_6-TiB_2 composites using the RSM method according to [29] allows one to assess the perfection of its crystal structure in composites [28]. During FZM crystallization, thermal and interfacial stresses result in the formation of a multilevel fragmented dislocation structure with high-angle boundaries (2-3°) between fragments and low-angle boundaries (0.05-0.5°) with excess dislocations inside them (109 cm^{-2}), forming bending deformations of the grains. This manifests itself in the shape and broadening $Iq_\perp$ of the intensity distributions of diffraction spots, as shown in Fig. 7a. The $Iq_\perp$ distributions are divided into separate areas with a non-uniform intensity distribution within them and different broadening. Multilevel structures contain high local stresses. Upon heating to 1200°C, the $Iq_\perp$ distributions gradually change, the misorientations in individual fragments are levelled, and the broadening of the diffraction spot decreases (Fig. 7b). When the composites are heated to 1600°C, the broadening of the $Iq_\perp$ distribution significantly decreases, the intensity becomes smooth in separate $Iq_\perp$ areas (Fig. 7c). This corresponds to perfection of the substructure of the matrix of composites, elimination of bending deformations, some decrease in misorientation between subgrains, and uniform distribution of dislocations within them.

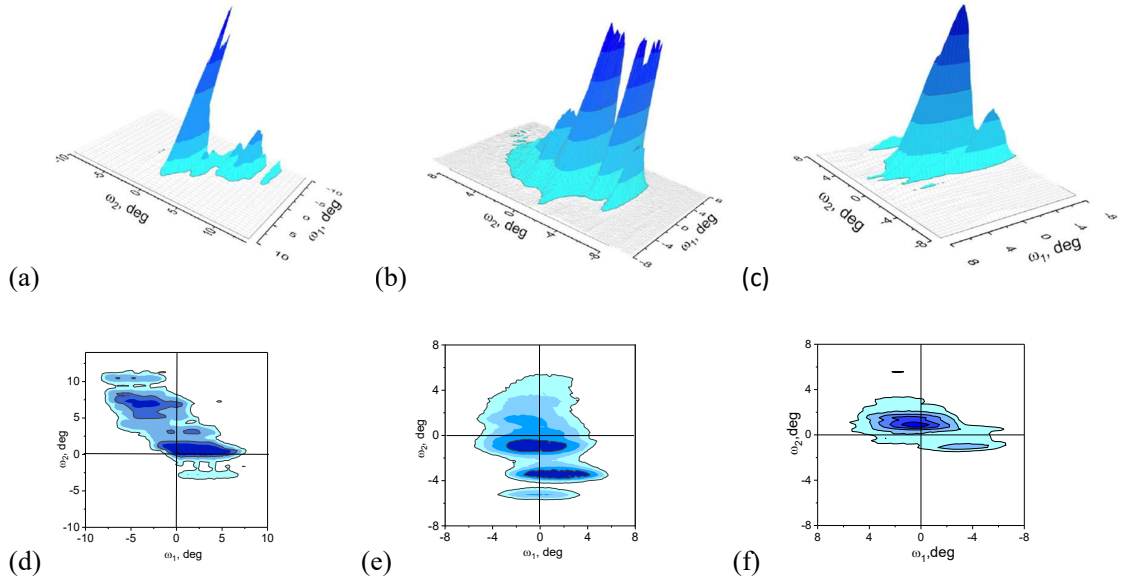

Fig. 7. (100) LaB_6 diffraction 3D (a, b, c) and 2D (d, e, f) $I_{q\perp}$ spots in LaB_6-TiB_2 composites. FZM state - a, d; after annealing at 1200°C - b, e; after annealing at 1600°C - c, f.

3.4. Thermal expansion coefficients of LaB_6-MeB_2 composites and LaB_6, MeB_2 borides

Based on the dilatometric data for short samples (the second heating curve), the CTE's of LaB_6-MeB_2 composites and LaB_6 ceramics were calculated [23], and, together with the literature data for MeB_2 borides, are presented in Fig. 8. The lines in Fig. 8 show experimental results for LaB_6 ceramics (Fig. 8a) and LaB_6-TiB_2 (Fig. 8b), LaB_6-HfB_2 (Fig. 8b), LaB_6-ZrB_2 (Fig. 8b) of the composites. The individual bullets represent CTE literature values for LaB_6, TiB_2, ZrB_2, HfB_2 in various crystallographic directions [21,23,24,37-43]. The CTE literature data of the diborides have a significant scatter, as they are a function of the crystallographic direction in a hexagonal crystal structure and also vary depending on the literature source and experimental procedure used to measure the CTE.

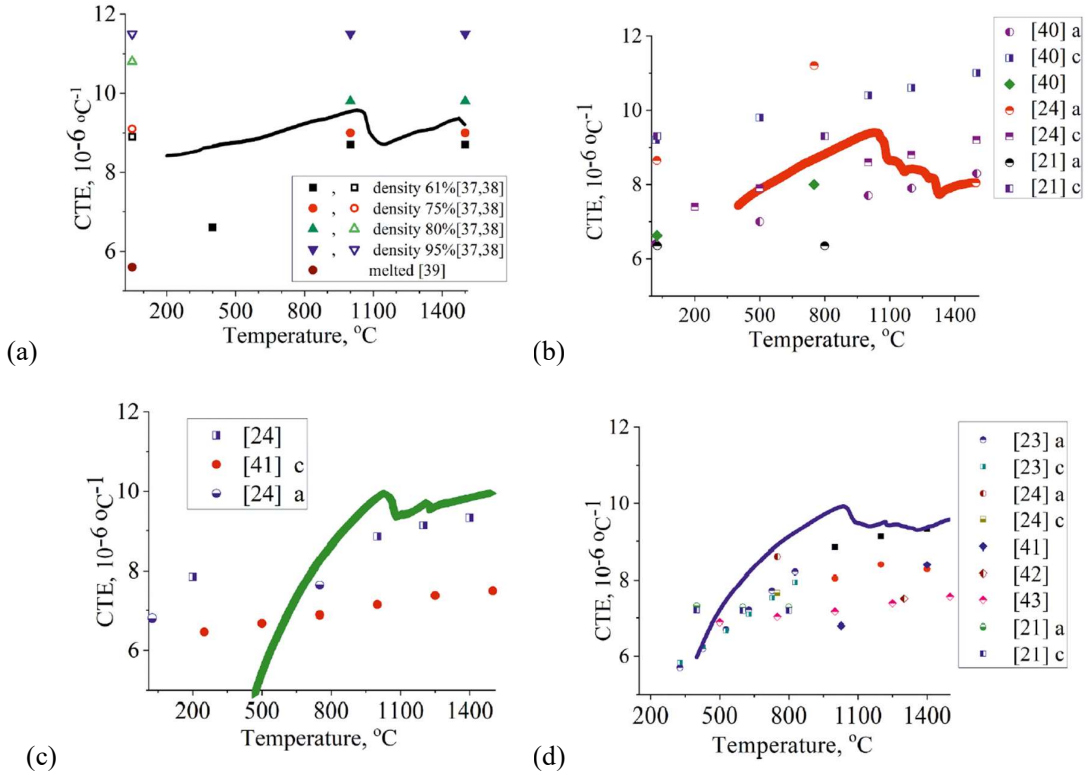

Fig. 8. The CTE values obtained in this work for LaB_6 hexaboride and LaB_6-MeB_2 composites (lines) and dots are the well-known CTE LaB_6 (MeB_2) borides. LaB_6 (a) [37-39], LaB_6-TiB_2 (b) [21,24,40], LaB_6-HfB_2 (c) [24,41] and LaB_6-ZrB_2 (d) [21,23,24,41-43].

The experimental CTE of LaB_6 almost linearly increases in the temperature range from 20 to 1000°C. A further increase in temperature results in a NCTE value falling in the temperature range ~1000-1200°C (Fig. 8a) and a linearly increasing positive CTE above this temperature interval. CTE values for LaB_6 with various density from literature data, represented in Fig. 8a. Change with temperature [37,38] and the actual differences are directly related to the LaB_6 density, i.e. the CTE increase with increasing density [39]. For LaB_6 single crystal grown by FZM, the existence of an anomalously small value of the elastic constant C12 (1.82), as compared to C11 (45.33), was experimentally shown, which leads to a crystallographic anisotropy of the CTE values [11]. A crystallographic anisotropy of the CTE caused by the anisotropy of softening of the atomic bonding was also predicted by theoretical studies [8,9,15]. However, averaging over orientations and insufficient density in polycrystals can mask the crystallographic temperature dependence of the experimental CTE in LaB_6.

The thermal expansion temperature dependency for LaB_6-MeB_2 composites can be arbitrarily divided into three areas: at low-temperature (<1000°C) with a monotonic increase in CTE, an intermediate temperature range (1000-1300°C) containing multiple NTE intervals, and a high-temperature range (>1300°C), with a monotonic increase in CTE. The lowest NCTE temperature range coincides with that for LaB_6 hexaboride, i.e. matrix of these composites. This suggests that the atomic bond softening occurs with an increase in temperature, primarily in the matrix. The subsequent NCTE temperature intervals are determined by the interatomic bond in MeB_2 diborides and between the matrix and reinforcing fibers. The largest scatter of the CTE values of the reinforcing (TiB_2) diborides as compared to the CTE of the composite is observed for the LaB_6-TiB_2 (Fig. 8b). This scatter exists both in the "a", "c" directions, and without indicating the direction, i.e. when averaging over orientations in polycrystalline samples. A smaller spread in the CTE data is inherent to the LaB_6-HfB_2 and LaB_6-ZrB_2 composites and the HfB_2 and ZrB_2 diborides (Fig. 8c, d).

The differences in CTE values of MeB_2 diborides are due to different Me radii, which resulting in changes in the length of the interatomic bonds [6,8-22,44]. More significant changes in MeB_2 diborides are observed for the "c" axis rather than for the "a" axis, due to the relative strength of the bonds Me-Me < Me-B < B-B. The minimum deformation of the boron network MeB_2 is observed at the "normal" b – b2 bond length (Fig. 1b) and is estimated as 1.74 Å [6]. In MeB_2, the shortest b-b2 bond length (1.75 Å) is observed for TiB_2 with the smallest atomic radius of the metal (Ti). Zr atom radius is larger than that of Ti and Hf, and the length of the b-b2 bond in ZrB_2 boride is 1.83 Å. Because of crystal-chemical reasons, the length of the "a" axis in borides is a balance between two forces: (1) repulsion between atoms of the Me layers and (2) attraction between atoms in the B-net. As a result, stable MeB_2-type diborides are not formed for atoms larger than Zr and smaller than Cr.

In the absence of phase interaction and texture, it can be expected that the CTE of LaB_6-MeB_2 composites will follow the simple rule of mixtures. However, in these composites, there is a clear connection between the matrix and the fibers and, therefore, their thermal expansion does not obey the rule of mixtures. In composites with thin fibers of the reinforcing phase and interatomic bonds different nature, NTE is observed due to softening of interatomic bonds, which is not determined by the Debye temperature for massive borides. The Debye's temperature for bulk materials is 920 K-1140 K for TiB_2, 510 K-742 K for ZrB_2, and 650 K-690 K for HfB_2 [18-21,44]. Influence of the MeB_2 borides on the composites' CTE can be estimated by comparing the CTE of the LaB_6 matrix and LaB_6-MeB_2 composites, as presented in Fig. 9.

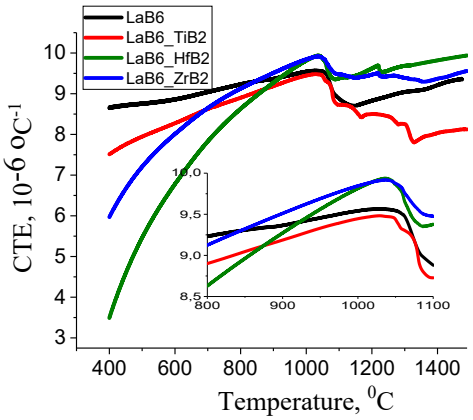

Fig. 9. Temperature dependency of the CTE of the LaB_6-MeB_2 composites and the LaB_6 matrix; 1-LaB_6, 2 -LaB_6-TiB_2, 3- LaB_6-HfB_2, 4 LaB_6-ZrB_2.

The CTE values of LaB_6 and LaB_6-MeB_2 composites coincide most closely for Me-Ti in comparison with other (Me-Zr, Hf) diborides. The LaB_6-TiB_2 CTE values does not exceed the CTE of LaB_6 matrix (Fig. 9, curves 1, 2). The CTE values of the LaB_6-ZrB_2 and LaB_6-HfB_2 composites (Fig. 9, curves 3, 4) in the low-temperature region are much lower than the CTE of LaB_6, but exceed this value at higher temperatures at ~830°C and ~920°C, respectively. Based on CTE data for all LaB_6-MeB_2 composites, their first NCTE interval coincides with the NCTE LaB_6 at 1000-1150°C. The number and value of the NCTE intervals vary for composites with different types of reinforcing fibers and are more pronounced for the LaB_6-TiB_2 compared to LaB_6-HfB_2 and LaB_6-ZrB_2.

Comparison of the LaB_6-MeB_2 CTE results with similar results on other composites, for example [5,45,46], causes us to consider coincidence of interplanar distances of phase components. Table 2 shows the values of the interplanar distances in the LaB_6 matrix and MeB_2 borides for 11 pairs of planes with the greatest symmetry and the smallest values of their mismatch. The smallest mismatch is observed in the LaB_6-TiB2 composite. Thus, a mismatch of ≤1% exists in the LaB_6-TiB_2 composite for the three matrix-fiber orientation ratios. Higher mismatches are present in LaB_6-ZrB_2 and LaB_6-HfB_2.

The smallest mismatch values are 1.65% and 2.58% for one pair of interplanar distances and 1.84% and 3.0% (after averaging over 3 planes with the minimum mismatch value) for LaB_6-ZrB_2 and LaB_6-HfB_2, respectively.

Different types of bonds (metallic, ionic, covalent) determine the hierarchy of interatomic interactions in the phase components of composites and cause softening in different temperature ranges. The presence of mismatch at the interface between the matrix and thin fibers enhances the differences in temperature dependences of the elongation and CTE of hexaboride and composites. The coherent coupling of the phase components of the composites determines the onset of softening of the initially weak La-La metal interatomic bond in the composite matrix. At the interphase boundaries of composites along the axis of samples with a polycrystalline structure and multidirectional fiber positions, there is a scatter of mismatch values. This can increase the difference in temperature ranges and NCTE values of LaB_6-MeB_2 composites with different types of fibers.

Table 2 Interplanar distances and mismatch of the LaB_6-MeB_2 components.

LaB_6 <hkl>	d_m LaB_6, Å (ICDD's PDF01-073-1669)	MeB_2 [hkl]	d_f ZrB_2, Å (ICDD's PDF 00-034-0423)	d_f HfB_2, Å (ICDD's PDF 00-012-0234)	d_f TiB_2, Å (ICDD's PDF 00-007-0275)	Mismatch, $(\eta d_m - \chi d_f)/d_m$, %			
						η/χ	ZrB_2	HfB_2	TiB_2
<100>	4.15686	[001]	3.53	3.47	3.24	1/1	15.08	16.52	22.06
		[111]	1.44547	1.431830	1.3707	1/3	4.32	3.33	1.07
		[101]	2.16632	2.142890	2.0354	1/2	4.23	3.1	2.07
		[102]	1.48453	1.464950	1.3745	1/3	7.14	5.72	0.80
		[100]	2.7445	2.72	2.62	2/3	1.93	3.7	10.9
<110>	2.93958	[100]	2.7445	2.72	2.62	1/1	6.6	7.4	10.8
		[110]	1.58428	1.572	1.515	1/2	7.79	6.95	3.07
		[111]	1.44547	1.431830	1.3707	1/2	1.65	2.58	6.7
<111>	2.3999	[001]	3.53	3.47	3.24	3/2	1.94	3.61	9.99
		[201]	1.278910	1.267130	1.2148	1/2	6.58	5.6	1.23
<210>	1.85899	[211]	0.995125	0.986295	0.9475	1/2	7.06	6.11	1.93
Mismatch over 1 plane (minimal)							1.65	2.58	0.80
Mismatch averaged over 2 planes with a minimum value							1.8	2.84	0.94
Mismatch averaged over 3 planes with a minimum value							1.84	3.0	1.03
Mismatch averaged over 8 planes with a minimum value							4.29	4.63	3.36

3.5. Thermal and mechanical properties of composites

The success of high-temperature employment of LaB_6-MeB_2 composites relies on the possibility of joint deformation of coherently coupled phase components based on the values of their CTE. From this point of view, the most acceptable reinforcement of lanthanum hexaboride is the use of MeB_2 fibers. However, in addition to the joint deformation of the matrix and the fibers, the strength of the composites depends on the amount of the reinforcing phase. In LaB_6-ZrB_2 composite volume of this phase is ~21 wt%, and ~11 wt%. in LaB_6-TiB_2 composite. In [5], it was proposed to replace a part of Zr with Ti in the LaB_6-ZrB_2 composite. Upon Ti doping, the length of the b-b2 bond in the $LaB_6Zr_xTi_yB_2$ composite began to decrease as compared to the LaB_6-ZrB_2 composite. The smallest discrepancy between the two boron sublattices (LaB_6 and $Zr_xTi_yB_2$) was found in the LaB_6 -$Zr0.4Ti_{0.6}B_2$ composite, where the b-b2 bond length in diboride was 1.760 Å and was close to the intraoctahedral B-B2 distance of 1.755 Å in the LaB_6 structure. When the interatomic distances in the boron sublattices of the two phases of the composite are comparable, the matrix and fibers phases are better coupled, the process of their joint deformation is facilitated and does not lead to the formation of cracks.

The strength and plasticity of composites react to RS and disoriented structures of composites [47]. The previous investigations show the ceramic composites flexural strength dependence on temperature [47-49]. Strength tests at low temperatures are carried out under high RS conditions, at local bending stresses of multilevel structures. Tests at high temperatures are performed at significantly reduced RS both for the LaB_6-MeB_2 composite and separately for its LaB_6 and MeB_2 phase components [28]. As a result, the strength in the high temperature range of tests (~0.5 Tm, melting temperature) increases as compared to the results at low-temperature deformation (Fig. 10). Preliminary annealing also improves the strength properties of the composites, with this temperature being ~1200°C for LaB_6-TiB_2 composite [27,47]. For the LaB_6-ZrB_2 composite, the strength begins to increase significantly at temperatures above 0.5 T_m [48-50]. For the HfB_2, the flexural stress at 1230°C is higher than at 1090°C [51].

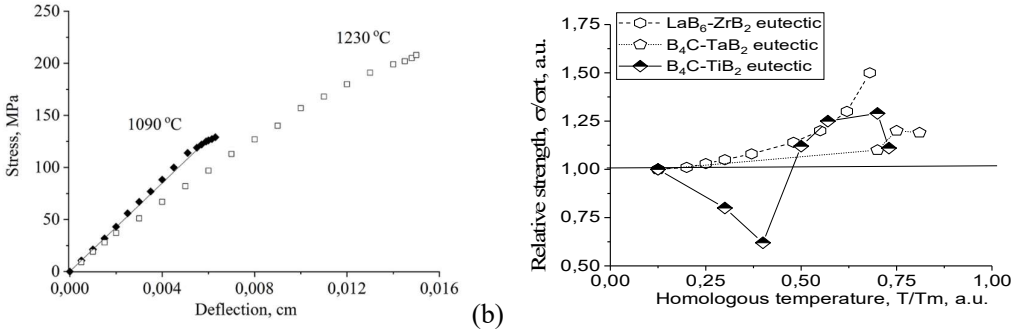

(a) (b)

Fig. 10. Flexural strength of HfB_2 (a) and ceramic composites (b) as a function of temperature [48-51].

In our opinion, an increase in the strength and plastic properties of LaB_6-MeB_2 composites is associated with interatomic bonds softening in their phase components. In the crystal sublattices of the matrix and reinforcing fibers, the amplitudes of atomic oscillations increase with increasing temperature. This leads to a significant increase in the concentration of equilibrium pairs of point defects of the Schottky - Frenkel type [52]. Point defects can migrate in the crystal lattice into the bulk of the material with local stresses. The boundaries and bends of the multilevel substructure and non-equilibrium phases are the centers of their adsorption. Point defects are added to the substructural components of composites, reduce local stresses, increase the mobility of dislocation defects, and create phase and structural equilibrium states. Composites with such a phase and structural state are deformed plastically, involving the matrix and fibers in this process. The NCTE intervals (1000-1250°C for LaB_6-MeB_2 composites) determine the transition from low-temperature deformation mechanism with brittle fracture of composites to a high-temperature mechanism with plastic deformation of its components.

4. Conclusions

1. In LaB_6-MeB_2 (Me-Ti, Zr, Hf) composites obtained by the FZM method, the temperature interval with a negative elongation are observed when heating in the temperature intervals from 20°C to 1500°C. The first such interval (~1000-1100°C) coincides in LaB_6-MeB_2 composites and LaB_6 hexaboride and is associated with La-La atomic bond softening in the matrix.

2. Thermal effects in coherently coupled phase components (LaB_6, MeB_2) of composites depend on the nature of the interatomic and interphase interaction (La-La, Me-B, B-B), the value of the mismatch between the matrix and reinforcing fibers, and on the non-equilibrium structural and phase states of the composites, reflecting also the crystallographic anisotropy of these properties.

3. The interatomic interactions softening in LaB_6-MeB_2 composites results in the appearance of NCTE and differs in temperature from similar bulk individual borides due to the interphase interaction coherence. The samples sizes of polycrystalline composites and reheating can affect the

manifestation of the temperature dependence of the interatomic interaction softening due to masking of this effect by averaging over crystallographic orientations and residual stresses.

4. The mismatch value of the coherent phase components of the composites in combination with the volume of the reinforcing phase determines the strength and ductility of LaB_6-MeB_2 composites.

5. Increasing high-temperature strength and fracture toughness of LaB_6-MeB_2 composites obtained under conditions of temperature gradients is caused by a decrease in RS and an improvement in the matrix substructure due to the formation of equilibrium pairs of Frenkel - Schottky point defects due to the interatomic interaction softening.

6. The NCTE intervals (1000-1250°C), associated with the softening of the interatomic bonds in the matrix and fibers, determine the change of the deformation mechanism of LaB_6-MeB_2 composites from low-temperature to high-temperature one.

Acknowledgements

The authors gratefully acknowledge the use of the services and facilities of the Department of Materials Engineering of KU Leuven. The authors thank P. Arras, T. Lapauw, S. Huang, I. Bogomol for their assistance with the experimental work.

References

[1] J. Voss, A. Vojvodic, S.H. Chou, R.T. Howe, F. Abild-Pedersen. Inherent enhancement of electronic emission from hexaboride heterostructure. Phys. Rev. Appl., 2 (2014),
[2] Q.H. Fan, Y.M. Zhao, D.D. Li. Synthesis of single-crystalline lanthanum hexaboride nanowires by Au catalyst. Ceram. Int., 39 (2013), pp. 6271-6275.
[3] P.I. Loboda. Structure and properties of reinforced ceramic materials produced by directional solidification. Powder Metall. Met Ceram., 57 (2018), pp. 13-26.
[4] H. Deng, E.C. Dickey, Y. Paderno. Crystallographic characterisation and indentation mechanical properties of LaB_6-ZrB_2 directionally solidified eutectics. J. Mater. Sci., 39 (2004), pp. 5987-5994.
[5] V. Filippov. The Nature of the Microstructure and Interface Boundary Formation in Directionally Solidified Ceramic Boride Composites. AFRL-AFOSR-UK-TR-2011-0016 (2011)
[6] F.-Z. Dai, Y.A. Zhou. Modified theoretical model of intrinsic hardness of crystalline solids (MeB_2). Sci. Rep., 6 (2016), p. 33085.
[7] F.M. Hossain, D.P. Riley, G.E. Murch. Ab initio calculations of the electronic structure and bonding characteristics of LaB_6. Phys. Rev. B, 72 (2005), p. 235101.
[8] D. Serebrennikov, Ev. Clementyev, P. Al. Alekseev. Analysis of the crystal lattice instability for cage–cluster systems using the superatom model. J. Exp. Theor. Phys., 123 (2016), pp. 452-460.
[9] Y.S. Ponosov, Shitsevalova. Phonons in YB_6 and LaB_6: effects of temperature and pressure. N.Y. JETP Lett., 102 (2015), pp. 295-300.
[10] F. Liu. Structure and chemical bond characteristics of LaB6. Physica B, 404 (2009), pp. 4086-4089.
[11] H.G. Smith, G. Dolling, S. Kunii, M. Kasaya, B. Liu, K. Takegahara, T. Kasuya, T. Goto. Experimental study of lattice dynamics in LaB_6 and YbB_6. Solid State Commun., 53 (1985), pp. 15-19.
[12] C.-H. Chen, Y. Xuan, S. Otani. Temperature and loading time dependence of hardness of LaB_6, YB_6 and TiC single crystals. J. Alloys Compd., 350 (2003), pp. L4-L6.
[13] L. Chao, L. Bao, W. Wei, O. Tegus, Z. Zhang. First-principles study on the electronic structure, phonons and optical properties of LaB_6 under high-pressure. J. Alloys Compd., 672 (2016), pp. 419-425.
[14] I. Mörke, P. Wachter. Phonon softening in intermediate valent SmB_6. J. Phys. Colloq., 42 (1981), pp. C6-C14-C6-16.
[15] X. Zeng, Y. Ye, S. Zou, Q. Gou, Y. Wen, P. Ou. First-Principles study of the nonlinear elasticity of rare-earth hexaborides REB_6 (RE = La, Ce). Crystals, 7 (2017), p. 320.

[16] D. Mandrus, B.C. Sales, R. Jin. Localized vibrational mode analysis of the resistivity and specific heat of LaB6. Phys. Rev. B, 64 (2001), Article 012302.
[17] M. Anisimov, V. Glushkov, A. Bogach, S. Demishev, N. Samarin, S. Gavrilkin, K. Mitsen, N. Shitsevalova, V. Filipov, S. Gabani, K. Flachbart, N. Sluchanko. Specific heat of $Ce_xLa_{1-x}B_6$ in the low cerium concentration limit. J. Exp. Theor. Phys. Lett., 116 (2013), pp. 760-765.
[18] Y. Zhou, H. Xiang, Z. Feng, Z. Li. General trends in electronic structure, stability, chemical bonding and mechanical properties of ultrahigh temperature ceramics TMB_2 (TM = transition metal). J. Mater. Sci. Technol., 31 (2015), pp. 285-294.
[19] D. Wiley, W.R. Manning, O. Hunter. Elastic properties of polycrystalline TiB_2, ZrB_2 and HfB_2 from room temperature to 1300 K. J. Less-Common Met., 18 (1969), pp. 149-157.
[20] A.L. Ivanovskii. Mechanical and electronic properties of diborides of transition 3d–5d metals from first principles: toward search of novel ultra-incompressible and superhard materials. Prog. Mater. Sci., 57 (2012), pp. 184-228.
[21] N.L. Okamoto, M. Kusakari, K. Tanaka, H. Inui, Sh. Otani. Anisotropic elastic constants and thermal expansivities in monocrystal CrB_2, TiB_2, and ZrB_2. Acta Mater., 58 (2010), pp. 76-84.
[22] V.V. Skripnyak, V.A. Skripnyak. Predicting the mechanical properties of ultra-high temperature ceramics. Lett. Mater., 7 (2017), pp. 407-411.
[23] W.A. Paxton, T.E. Özdemir, E. Favk, T. Whalen, H. Biçer, E. Koray, A. Lan, Z. Zhong, T. Tsakalakos. Anisotropic thermal expansion of zirconium diboride: an energy-dispersive X-ray diffraction study. J. Ceram. (2016), Article 8346563.
[24] F.G. Keih, E.J. Keplin. High-temperature thermal expansion of certain group IV and group V diborides. J. Am. Ceram. Soc., 50 (1967), pp. 81-84.
[25] W.-T. Chen, R.M. White, T. Goto, E.C. Dickey. Directionally solidified boride and carbide eutectic ceramics. J. Am. Ceram. Soc., 99 (2016), pp. 1837-1851.
[26] P.I. Loboda, H.P. Kysla, S.M. Dub, O.P. Karasevs'ka. Mechanical properties of the monocrystals of lanthanum hexaboride. Mater. Sci., 45 (2009), pp. 108-113.
[27] T.O. Soloviova, O.P. Karasevska, J. Vleugels, P.I. Loboda. Influence of annealing on crucible-free float zone melted LaB_6-TiB_2 composites. J. Alloys Compd., 729 (2017), pp. 749-757.
[28] T.O. Soloviova, O.P. Karasevska, P.I. Loboda.Structure, residual stresses and mechanical properties of LaB_6-TiB_2 ceramic composites. Ceram. Int., 45 (2019), pp. 8677-8683.
[29] M.A. Krivoglaz. Diffraction X-Ray and Thermal Neutron of Imperfect Crystals. Springer, Berlin-Heidelberg (1996).
[30] C. Chen, L. Zhang, et al. Characterization of LaB_6-ZrB_2 eutectic composite grown by the floating zone method. J. Cryst. Growth, 191 (1998), p. 873.
[31] M.C. Flemings. Solidification Process. McGraw-Jill, New York (1974).
[32] B. Basu, J. Humbeeck, O. Biest, J. Vleugels, L. Donzel, R. Schaller. Thermal expansion and damping characteristics of Y-TZP. Scripta Mater., 40 (1999), pp. 759-765.
[33] A. Laptev, B. Baufeld, A.K. Swarnakar, S. Zakharchuk, O. van der Biest. High temperature thermal expansion and elastic modulus of steels used in mill rolls. J. Mater. Eng. Perform., 21 (2012), pp. 271-279.
[34] M.E. Schlesinger, P.K. Liao, K.E. Spear. The B-La (boron-lanthanum) system. J. Power Electron., 20 (1990), p. 73.
[35] M.T. Dove, H. Fang. Negative thermal expansion and associated anomalous physical properties: review of the lattice dynamics theoretical foundation. Rep. Prog. Phys., 79 (2016), Article 066503.
[36] K. Takenaka. Negative thermal expansion materials: technological key for control of thermal expansion. Sci. Technol. Adv. Mater., 13 (2012), Article 013001.
[37] M.D. Williams, K.N. Leung, P. Purgalis. Lanthanum Hexaboride (LaB_6) Coefficient of Thermal Expansion. Lawrence Berkeley Laboratory, Preprint (1989).
[38] D.M. Goebela, R.M. Watkins. Compact lanthanum hexaboride hollow cathode. Rev. Sci. Instrum., 81 (2010), Article 083504.
[39] Comparing Lanthanum Hexaboride and Cerium Hexaboride Cathodes, EMS (Electron Microscopy Science) Catalog (2020). https://www.emsdiasum.com/technical/datasheet/80920.aspx
[40] R.G. Munro. Material properties of titanium diboride. J. Res. Natl. Inst. Stand. Technol., 105 (2000), pp. 709-720.

[41] J.W. Zimmermann, G.E. Hilmas, W.G. Fahrenholtz, R.B. Dinwiddie, W.D. Porter, H. Wang. Thermophysical properties of ZrB_2 and ZrB_2-SiC ceramics. J. Am. Ceram. Soc., 91 (2008), pp. 1405-1411.
[42] A. Bellosi, F.J. Monteverde. Hot structures and thermal protection systems for space vehicles. A. Wilson (Ed.), Proceedings of the 4th European Workshop Held 26-29 November, 2002 in Palermo, Italy, Paris: European Space Agency (2003). ESA SP-521.
[43] R. Loehman, E. Corral, H.P. Dumm, P. Kotula, R. Tandon. Ultra High Temperature Ceramics for Hypersonic Vehicle Applications. Sandia laboratory report (2006), p. 2925.
[44] W.G. Fahrenholtz, G.E. Hilmas, I.G. Talmy, J.A. Zaykoski. Refractory diborides of zirconium and hafnium. J. Am. Ceram. Soc., 90 (2007), pp. 1347-1364.
[45] E.N. Kablov, N.V. Petrushin. Physicochemical and technological features of creating metal-based high-superalloys. Pure Appl. Chem., 76 (2004), pp. 1679-1689.
[46] A.I. Samoulov, R.M. Nazarkin, N.V. Petrushin, N.S. Moiseeva. Mismatch as a Characteristic of the Level of Interfacial Stresses in Single-Crystal High-Temperature Nickel Alloys. VIAM (2011), p. 205748.
[47] O.P. Karasevska, T.O. Soloviova, Yu I. Bogomol, P.I. Loboda K. Abramov. Deformation of eutectic composite systems LaB_6-TiB_2 (ZrB_2). Metallofiz. Noveishie Tekhnol., 41 (2019), pp. 897-912.
[48] D. Demirskyi, O. Vasylkiv. Analysis of the high-temperature flexural strength behavior of B_4C-TaB_2 eutectic composites produced by in situ. Mater. Sci. Eng., 697 (2017), pp. 71-78.
[49] I. Bogomol, T. Nishimura, O. Vasylkiv, Y. Sakka, P. Loboda.The bending strength temperature dependence of the directionally solidified eutectic LaB_6-ZrB_2 composite. J. Alloys Compd., 509 (2011), pp. 6123-6129.
[50] I. Bogomol, T. Nishimura, O. Vasylkiv, Y. Sakka, P. Loboda. Microstructure and high-temperature strength of B_4C-TiB_2 composite prepared by a crucibleless zone melting method. J. Alloys Compd., 485 (2009), pp. 677-681.
[51] M. Opeka, I. Talmy, E. Wuchina, J. Zaykoski, S. Causey. Mechanical, thermal, and oxidation properties of refractory hafnium and zirconium compounds. J. Eur. Ceram. Soc., 19 (1999), pp. 2405-2414.
[52] C. Kittel. Introduction to Solid State Physics (8th, ed), Wiley (2004).